

Additional clock transitions in neutral ytterbium bring new possibilities for testing physics beyond the Standard Model

V. A. Dzuba¹, V. V. Flambaum¹, and S. Schiller²

¹*School of Physics, University of New South Wales, Sydney 2052, Australia and*

²*Institut für Experimentalphysik, Heinrich-Heine-Universität Düsseldorf, 40225 Düsseldorf, Germany*

We study the prospects of using transitions from the ytterbium ground state to metastable states $^3P_2^o$ at $E = 19710.388 \text{ cm}^{-1}$ and $4f^{13}5d6s^2 (J = 2)$ at $E = 23188.518 \text{ cm}^{-1}$ as clock transitions in an optical lattice clock. Having more than one clock transition in Yb could benefit the search for new physics beyond the Standard Model via studying the non-linearity of King's plot or the time-variation of the ratio of the frequencies of two clock transitions. We calculate the lifetime of the states, relevant transition amplitudes, systematic shifts, and the sensitivities of the clock transitions to a variation of the fine structure constant and to the gravitational potential. We find that both transitions can probably support ultra-high accuracy, similar to what is already achieved for the $^1S_0 - ^3P_0^o$ clock transition.

PACS numbers: 31.15.A-, 11.30.Er

I. INTRODUCTION.

The search for new physics beyond the Standard Model (SM) with low-energy experiments requires extremely accurate measurements. The highest fractional accuracy has been achieved for atomic optical clocks such as based on Sr, Yb, Al^+ , Hg, Hg^+ , and Yb^+ . It is now at the low- 10^{-18} level [1–7]. When clock transitions are also sensitive to new physics beyond the SM, the benefit of using atomic clocks is enormous. At least two clock transitions must be available in order to produce a test of the SM. The clock transitions must have different sensitivity to new physics to avoid cancellation of the effect in the ratio of frequencies. A good example of such a system is the Yb^+ ion. It has two clock transitions, one is an electric quadrupole (E2) transition between the ground $[\text{Xe}]4f^{14}6s^2 S_{1/2}$ and the excited $[\text{Xe}]4f^{14}5d^2 D_{3/2}$ states, another is an electric octupole (E3) transition between the ground and the excited $[\text{Xe}]4f^{13}6s^2 ^2F_{7/2}$ states. This second transition has high sensitivity to a variation of the fine structure constant [8] and to local Lorentz invariance violation [9], while the first transition can serve as an anchor.

It has been recently suggested that the search for a possible non-linearity of King's plot can be used in the search for new physics beyond the SM [10]. On a King's plot the ratios of isotope shifts for two atomic transition frequencies are plotted for several isotopes. In the absence of new physics all points are expected to be approximately on the same line (up to some small corrections [11]). Electron-nucleus interaction due to exchange of a hypothetical scalar particle produces a non-linearity of King's plot. The minimum data needed to search for non-linearity of King's plot requires two transitions and four isotopes (leading to three isotope shifts against a reference isotope). The expected smallness of the effect suggests the use of clock transitions.

The ytterbium atom has seven stable isotopes, one well-studied clock transition, and several metastable

states which can probably be used in additional clock transitions. In this paper we study the $[\text{Xe}]4f^{14}6s6p ^3P_2^o$ and $[\text{Xe}]4f^{13}5d6s^2 (7/2, 3/2)_2$ states. The numbers in parentheses are the angular momenta of the f -shell hole and of the d -electron. The subscript denotes the total electronic angular momentum $J = 2$.

The energy diagram for five lowest states of Yb is presented on Fig. 1. There are three metastable states and three transitions between ground and metastable states which can be used as clock transitions. The first (578 nm) transition is already used as clock transition in a number of laboratories around the world. In this work we study the other two clock transitions. The transition denoted by 1 - 4 in the following was first observed by Yamaguchi et al. [12], and has since been studied in the context of photoassociation and atom-atom interaction physics [13–15]. Transition linewidths in the kHz-range have been realized [16]. The 1 - 5 transition has not been studied experimentally yet, to the best of our knowledge.

II. CALCULATIONS.

We perform atomic structure calculations with the CIPT method [17]. It combines configuration interaction (CI) with the perturbation theory (PT) by treating excited configurations perturbatively rather than including them into the CI matrix. This reduces the size of the CI matrix for the many-electron problem by many orders of magnitude, making it possible to deal with systems having a large number of electrons outside closed shells. This is important for the current problem because we are dealing with states of ytterbium which have excitations from the $4f$ subshell. This means that the total number of external electrons is sixteen; e.g., in the excited $4f^{13}5d6s^2 (7/2, 3/2)_2$ state we have thirteen $4f$ electrons, one $5d$ electron and two $6s$ electrons.

The results for the energies of relevant low-energy states of Yb are presented in Table I. Note some small

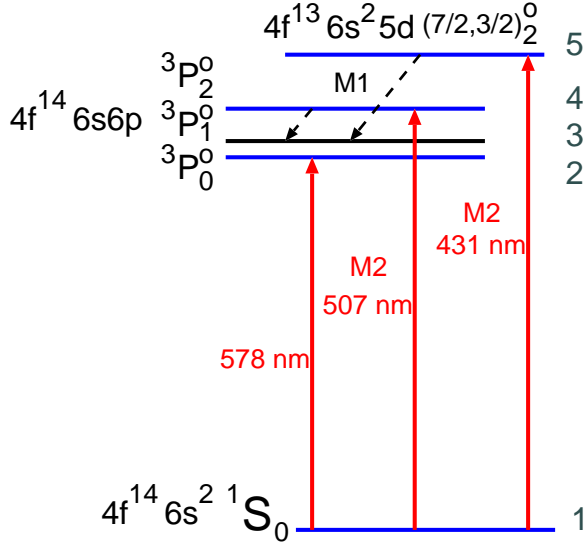


FIG. 1: Energy diagram for five lowest states of Yb (approximately to scale). Numeration of the states, presented on the right, is the same as in Table I. There are three metastable states and three clock transitions (1 - 2, 1 - 4 and 1 - 5). Dominating decay channels for clock states 4 and 5 are M1 transitions to the lower-lying $3P_1^o$ state.

TABLE I: Energies and lifetimes of low-lying states of Yb. New clock states are shown in bold.

N	State	J	Energy [cm ⁻¹]		Lifetime
			Expt. [18]	CIPT	
1	$4f^{14}6s^2 \ ^1S$	0	0	0	∞
2 ^a	$4f^{14}6s6p \ ^3P^o$	0	17288	17265	23-26 ^b s
3	$4f^{14}6s6p \ ^3P^o$	1	17992	18327	500 ns
4	$4f^{14}6s6p \ ^3P^o$	2	19710	19895	15^c s
5	$4f^{13}5d6s^2 \ (7/2, 3/2)^o$	2	23188	24831	200^c s
6	$4f^{13}5d6s^2 \ (7/2, 3/2)^o$	3	27445	27185	
7	$4f^{14}5d6s \ ^3D$	1	24489	27584	
8	$4f^{14}5d6s \ ^3D$	2	24751	27678	
9	$4f^{14}5d6s \ ^3D$	3	25271	27763	
10	$4f^{14}6s6p \ ^1P^o$	1	25068	24753	5 ns
11	$4f^{14}5d6s \ ^1D$	2	27677	28156	
12	$4f^{13}5d6s^2 \ (7/2, 5/2)^o$	1	28857	29610	8 ns

^aCurrent upper clock state.

^b23.0 s for ^{171}Yb and 26.0 s for ^{173}Yb [19].

^cFor even isotopes.

differences in the results compared to previous calculations [17]. This is due to differences in the basis and the size the effective CI matrix. These differences are within the accuracy of the method.

To calculate transition amplitudes we need to include the interaction of the atom with an external electromagnetic field. We consider the interaction in dipole and quadrupole approximation leading to electric and magnetic dipole (E1 and M1) and electric and magnetic quadrupole (E2 and M2) transitions. We use the random-phase approximation (RPA) for the interaction. The

RPA equations for single-electron atomic states have the form

$$(H^{\text{HF}} - \epsilon_c)\delta\psi_c = -(\hat{F} + \delta V^F), \quad (1)$$

where H^{HF} is the Hartree-Fock Hamiltonian, the index c enumerates states in the atomic core, $\delta\psi_c$ is a correction to the core state due to an external field, \hat{F} is the operator of the external field, and δV^F is the correction to the self-consistent Hartree-Fock potential due to the external field. Equations (1) are solved self-consistently for all states in the core, leading to the effective operator of the external field, $\hat{F} \rightarrow \hat{F} + \delta V^F$. Matrix elements between states containing external electrons are calculated by the formula

$$A_{ab} = \langle b || \hat{F} + \delta V^F || a \rangle, \quad (2)$$

where $|a\rangle$ and $|b\rangle$ are many-electron (sixteen for Yb) wave functions found in the CIPT calculations.

We consider interaction of atomic electrons with external field in dipole and quadrupole approximation leading to electric and magnetic dipole (E1 and M1) and electric and magnetic quadrupole (E2 and M2) transitions.

The rates of spontaneous emission are given in atomic units by

$$T_{E1,M1} = \frac{4}{3}(\alpha\omega)^3 \frac{A_{E1,M1}^2}{2J+1}, \quad (3)$$

for electric dipole (E1) and magnetic dipole (M1) transitions, and by

$$T_{E2,M2} = \frac{1}{15}(\alpha\omega)^5 \frac{A_{E2,M2}^2}{2J+1}, \quad (4)$$

for electric quadrupole (E2) and magnetic quadrupole (M2) transitions. In these formulae α is the fine structure constant, ω is the frequency (not angular frequency) of the transition in atomic units, A is the amplitude of the transition in atomic units, and J is the total angular momentum of the upper state. The magnetic amplitudes A_{M1} and A_{M2} are proportional to the Bohr magneton $\mu_B = |e|\hbar/2mc$. Its value in Gaussian-based atomic units is $\mu = \alpha/2 \approx 3.6 \times 10^{-3}$.

The calculated amplitudes and corresponding transition rates are presented in Table II. Note that the value of the electric dipole transition amplitude between states number 1 (ground state) and state number 10 (which is one of the transitions used for laser cooling of the Yb atom), $\langle 1 || E1 || 10 \rangle = 4.14$ a.u., is in excellent agreement with the experimental value of 4.148(2) a.u. [20]. This is in sharp contrast to the large disagreement between experiment and the value of 4.825 a.u. obtained in very sophisticated calculations treating the Yb atom as a two-valence-electron system [21]. The reason for this disagreement is the strong mixing between the $4f^{14}6s6p \ ^1P_1^o$ and $4f^{13}5d6s^2 \ (7/2, 5/2)_1^o$ states (states number 10 and 12 in Table I). This mixing cannot be properly taken into account in the two-valence-electrons approximation.

TABLE II: Transition amplitudes (A , in atomic units), corresponding rates (R) of spontaneous emission and experimental transition frequencies between some states of Table I. Numbers in square brackets indicate powers of ten. New clock transitions are shown in bold. To obtain A_{E2} , A_{M2} in SI units, multiply by $e a_0^2$.

Transition	Type	A	ω [cm^{-1}]	T [s^{-1}]
3 - 1	E1	0.711	17992	2.0[+6]
10 - 1	E1	4.14	25068	1.8[+8]
12 - 1	E1	2.71	28857	1.2[+8]
4 - 1	M2	0.61[-1]	19710	2.5[-4]
4 - 3	M1	0.57[-2]	1718	6.7[-2]
4 - 5	M1	0.37[-4]	3478	
5 - 1	M2	0.993[-2]	23188	1.5[-5]
5 - 2	E2	1.43	5900	3.3[-4]
5 - 3	M1	0.277[-3]	5196	4.7[-3]
5 - 4	M1	0.370[-4]	3478	2.6[-5]
5 - 6	M1	0.25[-2]	4257	
5 - 12	M1	0.49[-2]	5669	
7 - 5	E1	0.531[-1]	1301	
8 - 5	E1	0.186	1563	
9 - 5	E1	0.453	2086	
11 - 5	E1	0.744[-1]	4489	

See Ref. [21] for a detailed discussion. In current CIPT calculations we explicitly include mixing between three odd configurations, $4f^{14}6s6p$, $4f^{14}5d6p$, and $4f^{13}5d6s^2$, while all other configurations are included perturbatively.

In even isotopes the $^1S_0 - ^3P_0^o$ clock transition is extremely weak but can be opened by a magnetic field. The electric dipole amplitude between two states a and b induced by a magnetic field is

$$A_{B,ab} = \left(\sum_n \frac{\langle b|M1|n\rangle\langle n|E1|a\rangle}{E_b - E_n} + \sum_n \frac{\langle b|E1|n\rangle\langle n|M1|a\rangle}{E_a - E_n} \right) \times B. \quad (5)$$

Here B is the magnetic field directed along the z axis. The z components of the electric dipole and magnetic dipole matrix elements are used; the summation goes over the complete set of intermediate states. In the SI system, the atomic unit for magnetic field is 1 a.u. = 2.35×10^5 T. The transition rate is given by (3) while the angular frequency of the Rabi oscillations is $\Omega_R = E_0 A_{B,ab}$. Here E_0 is the amplitude of the laser electric field. Considering the $^1S_0 - ^3P_0^o$ (1 - 2) transition and using amplitudes from Table II for the three first contributions to eq. (5) we find that in SI units $\Omega_R/2\pi = (242 \text{ Hz/T} \sqrt{\text{mW/cm}^2}) B \sqrt{I}$. Here, I is the intensity of the laser wave. The coupling coefficient is in good agreement with the value $186 \text{ Hz/T} \sqrt{\text{mW/cm}^2}$ from Ref. [22].

TABLE III: Static scalar (α^S) and tensor (α^T) polarizabilities for Yb clock states, in atomic units. Numeration of the states is from Table I.

State	$\alpha^S(0)$	$\alpha^T(0)$
1	150	0
2	304	0
4	418	-70
5	124	-6

III. ANALYSIS

The calculated amplitudes and corresponding transition rates are presented in Table II. Using data from the Table we find that the lifetimes of the new clock states (number 4 and 5 in Table I) are about 15 s and 200 s respectively. This leads to the quality factors $Q = 2\pi\omega/R \approx 10^{16}$ and 10^{17} . The decay of these states is dominated by the M1 transitions to the $^3P_1^o$ state. The rates for the M2 transitions between these clock states and the ground state are $2.5 \times 10^{-4} \text{ s}^{-1}$ and $1.5 \times 10^{-5} \text{ s}^{-1}$, respectively. They are smaller than the rate of the hyperfine interaction-induced transition between clock state 2 ($^3P_0^o$) and the ground state, which varies between 10^{-2} and 10^{-1} s^{-1} depending on the isotope and the hyperfine structure components [19]. For comparison, they are larger than the rate of the hyperfine interaction-induced E3 transition in Yb^+ ions, which is $\sim 10^{-6} \text{ s}^{-1}$ [23].

A. Rabi oscillations.

In this paper we focus on even Yb isotopes to avoid large Zeeman shifts in M2 clock transitions (see below).

The Rabi frequency of a M2 transition is given by $\Omega_R = 2E_0 \alpha \omega A_{M2}$, (all values are in atomic units) Using the values of the M2 transition amplitudes from Table II we find $\Omega_R/2\pi = (88, 17) \text{ Hz} \sqrt{I}/\sqrt{\text{mW/cm}^2}$ for the 1 - 4 and 1 - 5 clock transition, respectively. The laser intensity I_π required to achieve a desired excitation time $T_\pi = \pi/\Omega_R \simeq 1 \text{ s}$ is of order $\mu\text{W/cm}^2$ and lower, a very small value.

B. Polarizabilities, black-body radiation and Stark shifts.

The shifts of the clock frequency due to the effect of black-body radiation (BBR), of the lattice laser field that traps the atoms, and of the clock laser field depend on the dipole polarizabilities of the clock states.

The total dipole polarizability of a state with angular momentum $J \geq 1$ in a laser field of frequency ω_L , linearly polarized and parallel to the quantization direction is [24]

$$\alpha(\omega_L) = \alpha^S(\omega_L) + \frac{3J_z^2 - J(J+1)}{J(2J-1)} \alpha^T(\omega_L), \quad (6)$$

where α^S and α^T are the dynamic scalar and tensor dipole polarizabilities, respectively and J_z is the projection of J . More general polarization geometries are treated later in section V A 1. States 1 and 2 have $J = 0$ (or, in case of fermionic isotopes with nuclear spin $1/2$, $F = 1/2$), thus $\alpha^T \equiv 0$. For states 4 and 5, $J = 2$, and α depends on J_z :

$$\alpha_a = \alpha^S - \alpha^T, \text{ for } J_z = 0, \quad (7)$$

$$\alpha_a = \alpha^S - \alpha^T/2, \text{ for } J_z = \pm 1, \quad (8)$$

$$\alpha_a = \alpha^S + \alpha^T, \text{ for } J_z = \pm 2. \quad (9)$$

The polarizabilities of an atomic state a with angular momentum J are given by

$$\alpha_a^S(\omega_L) = \frac{2}{3(2J+1)} \sum_n \frac{(E_n - E_a) \langle a | \hat{D} | n \rangle^2}{(E_n - E_a)^2 - \omega_L^2}, \quad (10)$$

$$\alpha_a^T(\omega_L) = 2 \sqrt{\frac{10J(2J-1)}{3(2J+3)(2J+1)(J+1)}} \times \quad (11)$$

$$\sum_n (-1)^{J+J_n} \left\{ \begin{matrix} 1 & 1 & 2 \\ J & J & J_n \end{matrix} \right\} \frac{(E_n - E_a) \langle a | \hat{D} | n \rangle^2}{(E_n - E_a)^2 - \omega_L^2},$$

where the summation goes over the complete set of excited many-electron states, \hat{D} is the operator of the electric dipole interaction in the valence space, $\hat{D} = \sum_v (d_v + \delta V_v)$. Here $d_v = -er_v$, δV_v is the RPA correction to the electric dipole operator acting on electron v (see eqs. (1,2)), and the summation over v is the summation over the valence electrons. There are also core and core-valence contributions to the scalar polarizability. We calculate them as described in Ref. [25].

The polarizabilities are well-known for the ground and the $^3P_0^o$ states (see, e.g. [21, 26]). There are also experimental and theoretical studies of the polarizabilities of state 4 [12, 27, 28]. However, we are not aware of any calculations or measurements for state 5. We perform the calculations for all clock states, 1, 2, 4 and 5 using two different approaches. States 1, 2 and 4 are the states with two valence electrons above the closed $4f$ shell. Therefore, we apply a well-developed techniques to perform the calculations (see, e.g. [21, 25]).

State 5 has a hole in the $4f$ subshell and requires a different treatment. In principle, one can directly use expressions (10) and (11), substituting experimental energies and calculated electric dipole matrix elements. This is useful at least for checking the contributions of low-lying resonances. However, it does not give correct polarizability due to a large contribution of the highly excited states, e.g. of the $4f^{13}5d6s6p$ configuration. Inclusion of highly excited states in the CIPT method is computationally very expensive. Therefore, in addition to direct summation, we use an approach developed in Ref. [30] for atoms with open f -shells. It uses the fact that polarizabilities of such atoms are dominated by matrix elements between states with the same $4f^n$ or $5f^n$ subshell, i.e. excitations from the f -shell can be ignored.

TABLE IV: Computed polarizabilities at the clock transition frequencies, differential polarizabilities $\Delta\alpha$ and corresponding frequency shift coefficients due to intensity of the probe laser. It is assumed for states 4 and 5 that $\alpha_a = \alpha_a^S - \alpha_a^T$.

Transition	ω_L (cm ⁻¹)	$\alpha_1(\omega_L)$ (a.u.)	$\alpha_a(\omega_L)$ (a.u.)	$\Delta\alpha_{a1}(\omega_L)$ (a.u.)	Stark shift (Hz cm ² /W)
1 - 2	17288	315	6	-310	15
1 - 4	19710	355	< 10 ³	< 10 ³	< 10 ²
1 - 5	23189	961	< 10 ³	< 10 ³	< 10 ²

In our case this means that the $4f^{13}$ subshell is treated as a closed shell with occupation number 13/14. Then the remaining valence electrons form the $6s^25d^2D_{3/2}$ state similar to the ground state of Lu. The polarizabilities are calculated as for a three-valence-electron system having the $6s^25d^2D_{3/2}$ ground state. This approach gives reasonably good results at least at some distance from resonances [30]. We do not calculate the polarizabilities of state 5 beyond first resonance (at $\omega \sim 0.04$ a.u.) because closeness to resonances makes calculations in this region unreliable.

The results are presented in Tables III and IV and further discussed in section V A 1. Static polarizabilities ($\omega_L = 0$) are presented in Table III. "Magic" frequencies occur when the polarizabilities of the two clock states are equal so that the frequency of the transition is not sensitive the electric field strength of the lattice wave. The magic frequencies are discussed in section V A 1.

Earlier polarizability calculations were performed in refs. [12, 13, 21, 26–28]. In particular, Khramov et al. [28] predicted magic wavelengths for the 1 - 4 transition based on calculated polarizabilities.

Our results for states 1, 2 and 4 are in good agreement with the earlier calculations and with available experimental data. E.g., our value for the difference of static polarizabilities of states 1 and 2, $\Delta\alpha(0) = 154$ a.u. (see Table III) differs by less than 6% from the experimental values $\Delta\alpha(0) = 146.1(1.3)$ a.u. [4] and $\Delta\alpha(0) = 145.726(3)$ a.u. [29]. The ratios of the polarizabilities of state 4 for $J_z = 0, -1, -2$ to the polarizability α_1 of the ground state 1, were measured in Ref. [28] at the laser wavelength $\lambda = 1064$ nm. Our calculated values for these ratios, $\alpha_4(J_z = 0)/\alpha_1 = 1.35$, $\alpha_4(J_z = -1)/\alpha_1 = 1.06$, $\alpha_4(J_z = -2)/\alpha_1 = 0.20$, agree well with the experimental values 1.6(2), 1.04(6), and 0.20(2) [28].

For the BBR shift it is sufficient to consider the difference in polarizabilities $\Delta\alpha_{ab}(0)$ of the two clock states at zero frequency. For the 1 - 4 clock transition $\Delta\alpha_{41}(0) = 268$ a.u. (see Table III). This is approximately 1.7 times larger than for the 1 - 2 transition. Correspondingly, the BBR shift is also 1.7 times larger, i.e. $\Delta\omega_{\text{BBR},14} \simeq 1.7$ Hz at 300 K [21]. In contrast, the BBR shift of the 1 - 5 clock transition is about 6 times smaller, $\Delta\omega_{\text{BBR},15} \simeq 0.2$ Hz at 300 K.

We may thus expect that for both new clock transitions the BBR shifts can be controlled, respectively, at the

same level as or better than that for the current Yb clock transition 1 - 2, 1×10^{-18} [4].

We now estimate the clock transition Stark shift due to the clock laser electric field ("probe shift"). It is given by (in atomic units)

$$\Delta\omega_p \approx -\Delta\alpha_{ab}(\omega_L) \left(\frac{\varepsilon_p}{2}\right)^2, \quad (12)$$

where ε_p is the amplitude of the clock laser electric field. Computed polarizabilities and corresponding Stark shifts of the clock transitions are listed in Table IV. The number for the 1 - 2 transition is in exact agreement with the result of Ref. [22]. In contrast, for the 1 - 4 and 1 - 5 transitions we can only give rough estimations. This is because calculations become unreliable when frequency comes close to a resonance. At $\omega_L = E_a$ resonance contributions come from states with $E_n \approx 2E_a$ which satisfy electric dipole selection rules for the $n - a$ transition. There are four states of the $4f^{14}6s5d$ configuration with energies 39 808, 39 838, 39 966 and 40 061 cm^{-1} which give dominant contribution to the polarizability of state 4, and there are four states of the $4f^{13}5d6s6p$ configuration with energies $E_n=45\,338$, 45 595, 46 395, and 46 431 cm^{-1} which give dominant contribution to the polarizability of state 5. Assuming that the amplitude is ~ 1 a.u. and using Eq. (10) we get $\alpha_5^S(\omega_L) < 10^3$ a.u.

Finally, we briefly consider the relevance of static Stark shifts stemming from the electric field produced by undesired stray charges on the windows of the vacuum chamber. In the field of lattice clocks it is known how to measure these so that the d.c. Stark shift uncertainty is at the 10^{-18} level for Yb, and also for Sr. Therefore, we only need to discuss the Stark shift coefficients $\Delta\alpha_{ab}(0) = \alpha_a(0) - \alpha_b(0)$ of the proposed transitions and compare them with that of the conventional clock transition. Table III shows that $\Delta\alpha_{ab}(0)$ for the 1 - 4 transition is similar to that of the conventional 1 - 2 transition. On the other hand, as mentioned above, for the 1 - 5 transition it is significantly smaller. Thus, there is no critical systematic shift issue here.

C. Zeeman shifts.

The clock states considered in this work have the relatively large value of the total electronic angular momentum $J = 2$. This means that they could be sensitive to external magnetic field and electric field gradients. We can consider fermionic and bosonic Yb atoms.

With fermionic isotopes, the total atomic angular momentum F will be half-integer and thus there will be no states with zero total spin projection F_z . For lattice clocks with fermionic isotopes, it is a standard experimental practice to cancel the first-order Zeeman shift by alternately probing two transitions with opposite values of $F_{z,a} - F_{z,b}$ and averaging the two transition frequencies. However, the Zeeman shift in the standard 1 - 2 transition is a nuclear Zeeman shift. In the

present transitions 1 - 4, 1 - 5, the electronic Zeeman shift occurs, with electronic Landé factor $\simeq 1.5$ and shifts $\approx (10 \text{ GHz/T}) \times F_{z,a}$. In order to achieve an uncertainty of the residual first-order shift equal to 1×10^{-18} on either transition, the uncertainty of the magnetic field variation between the alternating measurements must be $\leq 6 \times 10^{-10} \text{ G}/F_{z,a}$, not necessarily on the time scale between interrogations (several seconds) but over an appropriate averaging time interval. It will be difficult to achieve this, although the availability of several Zeeman states F_z and two clock transitions may help to devise appropriate strategies.

All bosonic Yb isotopes, including the radioactive ones with macroscopic lifetimes, have nuclear spin 0. Thus, the two clock states 4 and 5 have nonzero $F = J = 2$. From the point of view of Zeeman shifts, the bosonic isotopes are advantageous, since levels 4, 5 as well as the ground state offer $F_z = J_z = 0$ states. The first-order Zeeman shift is then absent for transitions between such states. Therefore, we shall focus on the bosonic isotopes in the following.

The quadratic Zeeman shift can be estimated using second-order perturbation theory,

$$\delta E_Z(J, J_z) = \sum_n \frac{|\langle n, J_n, J_z | \mu_z H_z | J, J_z \rangle|^2}{E_J - E_n}, \quad (13)$$

where $J_n = J, J \pm 1$ and the summation goes over the complete set of states. In most cases, the summation is strongly dominated by terms within the same fine-structure multiplet. This is because of small energy denominator and large value of magnetic dipole matrix elements. However, for clock state number 5 (see Table I) three states give significant contribution, states number 6, 10 and 12. The first two are within the same fine structure multiplet as clock state 5, while state 12 is strongly mixed with state 10. The Zeeman shifts calculated for the three clock states are presented in Table V. There are several things to note:

(1) The largest shift coefficient is for the $^3P_0^o$ state. This is due to the small fine structure interval of 704 cm^{-1} between the $^3P_0^o$ and $^3P_1^o$ states.

(2) $J_z = 0$ states of levels 4 and 5 have shifts smaller than that of the conventional level 2.

(3) For state 4 the quadratic shift is extremely small for $J_z = \pm 2$ because there is no mixing with this state within the fine-structure multiplet. The shift is due to the M1 matrix elements with states of different configurations. Such matrix elements are very small due to the orthogonality of the wave functions. The shift is further suppressed by large energy denominators.

(4) For state number 5 the shift coefficient for $J_z = \pm 2$ is also small. This may be convenient if such states are used for particular purposes where suppression of linear Zeeman shift is aimed for.

The quadratic Zeeman shift for the ground state is small, since there are no fine-structure contributions. It is much smaller than for the upper clock states and can be neglected in the difference.

TABLE V: Second-order Zeeman shift coefficient for clock states, in units Hz/G². J_n denotes the contributing states.

State	J	J_n	J_z	Shift		
				This work	Other	
2	0	1	0	-6.0[-2]	-6.2[-2] ^a	-7(1)[-2] ^b
4	2	1,2,3	0	1.2[-2]		
			1	9.2[-3]		
			2	-4.7[-7]		
5	2	1,2,3	0	-4.3[-3]		
			1	-3.4[-3]		
			2	-3.4[-3]		

^aTheoretical estimation, Ref. [22].

^bExperiment, Ref. [32].

D. Electric quadrupole shift.

The energy shift due to a gradient of a residual static electric field ε is described by a corresponding term in the Hamiltonian

$$\hat{H}_Q = -\frac{1}{2}\hat{Q}\frac{\partial\varepsilon_z}{\partial z}, \quad (14)$$

where \hat{Q} is the atomic quadrupole moment operator ($\hat{Q} = |e|r^2Y_{2m}$, the same as for E2 transitions). The energy shift of a state with total angular momentum J is proportional of the atomic quadrupole moment of this state. It is defined as twice the expectation value of the \hat{Q} operator in the stretched state

$$Q_J = 2\langle J, J_z = J | \hat{Q} | J, J_z = J \rangle. \quad (15)$$

Calculations similar to those described above give the values $Q_J = -18$ a.u. for state 4, and $Q_J = -5.3$ a.u. for state 5. For a state with projection J_z of the total angular momentum J , the shift is proportional to $3J_z^2 - J(J+1)$. Note that if $J = 2$ the shift has the same value, but opposite sign, for $J_z = 0$ and $J_z = \pm 2$. Therefore, averaging over these states can, at least in principle, suppress both electric quadrupole and linear Zeeman shifts. In addition, the vector light shift and the tensor light shift cancel (not the scalar).

Alternatively, it is possible to reduce the quadrupole shift by measuring the transition frequency three times, with the magnetic field direction applied in three mutually orthogonal directions [31]. In this case one can use only states with $J_z = 0$ avoiding the linear Zeeman shift.

E. Search for variation of the fine structure constant.

To search for a possible time variation of the fine structure constant α one needs to monitor a ratio of two clock frequencies i, j over a long period of time. Atomic calculations are needed to link a variation of frequencies to a variation of α . It is convenient to express the atomic

TABLE VI: Sensitivity of Yb clock transitions to variation of the fine structure constant. Transition frequencies are experimental.

Clock transition	Transition frequency ω_0 (cm ⁻¹)	q (cm ⁻¹)	$K = 2q/\omega_0$
1 - 2	17288.439	2714 ^a	0.31
1 - 4	19710.388	5505	0.56
1 - 5	23188.518	-44290	-3.82

^aRef. [8].

transition frequencies in a form

$$\omega = \omega_0 + q \left[\left(\frac{\alpha}{\alpha_0} \right)^2 - 1 \right], \quad (16)$$

where ω_0 and α_0 are present-time values of the frequency and the fine structure constant, and q is the sensitivity coefficient which comes from calculations. Then

$$\frac{\partial}{\partial t} \ln \frac{\omega_i}{\omega_j} = \frac{\dot{\omega}_i}{\omega_i} - \frac{\dot{\omega}_j}{\omega_j} = \left(\frac{2q_i}{\omega_i} - \frac{2q_j}{\omega_j} \right) \frac{\dot{\alpha}}{\alpha}. \quad (17)$$

To find the values of q for each transition we calculate the frequencies of the transitions at different values of α and then calculate the derivative numerically. The values of q and corresponding enhancement factors $K = 2q/\omega_0$ are presented in Table VI. We see that the 1 - 5 transition is the most sensitive to the variation of the fine structure constant. If we compare it to the currently used 1 - 2 transition then

$$\frac{\dot{\omega}_{15}}{\omega_{15}} - \frac{\dot{\omega}_{12}}{\omega_{12}} = 4.12 \frac{\dot{\alpha}}{\alpha}. \quad (18)$$

In other words, there is significant enhancement of the variation of the frequency ratio compared to the variation of the fine structure constant. The enhancement comes from the different nature of the two clock transitions. The clock transition 1 - 2 corresponds to the $s - p$ single-electron transition, while the clock transition 1 - 5 is the $f - d$ transition.

The figure of merit F_{ij} associated with a particular transition pair i, j is the ratio of α -sensitivity to the (absolute) systematic uncertainty u of the frequency ratio,

$$F_{ij} = \frac{|K_i - K_j|}{u(\omega_i/\omega_j)} = \frac{|2q_i/\omega_i - 2q_j/\omega_j|}{\sqrt{(u(\omega_i)/\omega_i)^2 + (u(\omega_j)/\omega_j)^2}}. \quad (19)$$

We note that the uncertainties of the transitions, $u(\omega_i)$, $u(\omega_j)$, do not possess any natural proportionality to their respective transition frequencies. Therefore, if one of the transition frequencies is significantly smaller than the other, no particular advantage results. At the present level of analysis of the systematic shifts, it appears that comparing the optical transitions 1 - 2 and 1 - 5 would be as performant as the comparison of 1 - 2 and the infrared transition 2 - 5 proposed in Ref. [33] (see also discussion in Section IV).

F. Search for Einstein Equivalence Principle violation.

Theories attempting the unification of gravity with other interactions suggest that the Einstein equivalence principle (EEP) might be violated at high energy [34]. It might be possible to discover evidence for the violation at low energies by observing tiny variations of atomic frequencies in a varying gravitational potential. High-precision atomic clocks can be used to search for such variations [35]. In the framework of the Standard Model Extension (SME), the term in the hamiltonian responsible for the EEP violation can be presented in the form (see, e.g. [36, 37])

$$\hat{H}_{c00} = c_{00} \frac{2}{3} \frac{U}{c^2} \hat{K}, \quad (20)$$

where c_{00} is one of the parameters in the SME characterising the magnitude of the EEP violation, U is the gravitation potential, c is the speed of light, $\hat{K} = c\gamma_0\gamma^j p_j/2$ is the relativistic operator of kinetic energy in which γ^j are Dirac matrices, and $\mathbf{p} = -i\hbar\nabla$ is electron momentum operator. Upper limits for c_{00} can be determined experimentally by measuring the frequency ratio of two dissimilar, co-located clocks, as a function of the local gravitational potential U ,

$$\frac{\omega_j}{\omega_i} \Delta \left(\frac{\omega_i}{\omega_j} \right) = \frac{\Delta\omega_i}{\omega_i} - \frac{\Delta\omega_j}{\omega_j} = -(R_i - R_j) \frac{2}{3} c_{00} \frac{\Delta U}{c^2}. \quad (21)$$

R_i are relativistic factors which describe the deviation of the expectation value of the kinetic energy E_K from the value given by the virial theorem (which states $E_K = -E$, where E is the total energy),

$$R_{ba} = - \frac{E_{K,a} - E_{K,b}}{E_a - E_b}. \quad (22)$$

ΔU is the change of the gravitational potential between the measurements. Experimentally, one should make several measurements during at least one year and search for a correlation between atomic frequency ratio and the Earth-Sun distance (see [35] for details).

One needs two atomic transitions with different values of R . Both the size $|R_i - R_j|$ and the experimental inaccuracies of the determination of the two frequencies ω_i , ω_j are critical parameters determining the sensitivity of the test, analogously to the earlier discussion.

The value of R can be found from relativistic atomic calculations. For the 1 - 2 clock transition it was calculated in Ref. [35], $R_{12} = 1.20$. Transitions which are sensitive to a variation of the fine structure constant should have relativistic factors significantly different from the non-relativistic limit $R = 1$. We calculated the relativistic factors for the 1 - 4 and 1 - 5 clock transitions using the approach of Ref. [35] and the CIPT method. The results are $R_{14} = 1.40$ and $R_{15} = 0.62$. These values imply a good sensitivity to the EEP-violating term in eq. (20).

For example, if the frequencies of the 1 - 2 and 1 - 5 transitions are compared, then

$$\frac{\Delta\omega_{12}}{\omega_{12}} - \frac{\Delta\omega_{15}}{\omega_{15}} = -0.37c_{00} \frac{\Delta U}{c^2}. \quad (23)$$

This value of $|R_i - R_j|$ is higher than for most other optical clock transitions (with exceptions of Yb^+ and Hg^+) [35].

G. Search for new physics using the non-linearity of King's plot.

In the King's plot the isotope shift of an atomic transition is plotted against the isotope shift of another transition. This is done for several isotopes with every new isotope adding a new point on the plot. Normally, all points are on the same line. This is a consequence of the factorisation of the nuclear and electron variables in the field (volume) shift term. See Ref. [38] for the case of Yb. However, if there is a new interaction between atomic electrons and nucleus which depends on the number of neutrons, the factorisation and thus linearity might be broken. The expected small value of the hypothetical effect demands for a high accuracy of the measurements. Therefore, it is best to use clock transitions.

The ytterbium atom has seven stable isotopes, two of them have non-zero nuclear spin. The choice of isotope depends on whether the hyperfine interaction is needed to induce the transition. This is an issue for the clock transition 1 - 2 which is the transition between states of zero total angular momentum. It is forbidden in the absence of hyperfine structure (see, e.g. [19]) or of external field. For that reason the ^{171}Yb isotope which has nuclear spin $I = 1/2$ is usually used for the clock. In the context of the present study, we do not consider odd isotopes, since in the states 4 and 5 they only possess $F_z \neq 0$ sub-states with very large linear (electronic) Zeeman effect.

We consider instead isotopes with zero nuclear spin (bosonic Yb), noting that it has recently been shown that high clock accuracy can also be reached with such isotopes and the $^1\text{S}_0 - ^3\text{P}_0^\circ$ transition in the strontium system [39–41].

Since we need at least four isotopes, there are the following possibilities: (1) Use only M2 clock transitions (transitions 1 - 4 and 1 - 5) in even isotopes. (2) Use magnetic-field induced spectroscopy of the $^1\text{S}_0 - ^3\text{P}_0$ transition in the four even isotopes with no nuclear spin. Use either of the two M2 transitions as the second clock transition, in the same isotopes.

IV. COMPARISON WITH OTHER CALCULATIONS

During completion of our work a paper by Safronova *et al* on the similar subject appeared [33]. The authors consider another clock transition in Yb, between states 2

and 5, and suggest it for a $\dot{\alpha}$ search. There is some overlap between their work and the present one and generally reasonably good agreement between overlapping results. E.g., the sensitivity of state 5 to variation of α is in very good agreement. There are some differences too, in particular in the values of the transition amplitudes and in the lifetime of state 5. A detailed comparison between the theoretical approaches is not possible, since not all details are reported in [33]. Some preliminary comments are as follows.

Ref. [33] claims the finding of the clock transition with the highest sensitivity to the variation of α . Indeed, the value of the enhancement factor is large, $K = 2\Delta q/\omega_{25} = -16$ (see Table VI for the numbers) and this is due to small value of ω_{25} .

We note that comparing only the enhancement factors for different atomic transitions may lead to wrong conclusions because the enhancement factor and the fractional measurement uncertainty of the frequency $u(\omega)/\omega$ are equally important. This has been discussed above. As an example, consider the largest known enhancement factor $K \sim 10^8$ for a transition in Dy [42, 43]. The limit on the time-variation of α obtained with the use of this transition ($\sim 10^{-17} \text{ yr}^{-1}$ [43]) is not stronger than those obtained in systems with $K \sim 1$ [44, 45]. This is because the relative uncertainty $u(\omega)/\omega$, is also large in Dy.

When possible, including the case of the 1 - 5 and 2 - 5 transitions in Yb, it is more instructive to compare the ratios $2\Delta q/u(\omega)$, as may be inferred from eq. (19). Δq is similar for both transitions ($-44\,290 \text{ cm}^{-1}$ for the 1 - 5 transition and $-44\,290 - 2\,714 = -47\,004 \text{ cm}^{-1}$ for the 2 - 5 transition, see Table VI). The uncertainty $u(\omega)$ is also likely to be similar, because both transitions use state 5, which is the more likely source of dominant uncertainty, due to the state's complicated structure. Therefore, both transitions will probably have a similar figure of merit for testing $\dot{\alpha}$.

In our opinion, the 1 - 5 transition has the advantage of being a transition from the ground state, which is experimentally simpler.

The good agreement for the α sensitivity between the present calculation and ref. [33] is due to the fact that it is not sensitive to the incompleteness of the basis. Indeed, the relativistic energy shift of a single-electron basis state can be approximated by the formula [46]

$$\Delta E_\nu \approx -\frac{1}{2\nu^3} (Z\alpha)^2 \left(\frac{1}{j+1/2} - C \right), \quad (24)$$

where ν is the effective principal quantum number ($E = -1/2\nu^2$), j is the total angular momentum of the state and C is a fitting parameter to simulate the many-body effects ($C \approx 0.6$). High basis states (large ν) have small relativistic energy shift and contribute very little to the relativistic energy shifts (parameters q in eq. (16)) of the low-lying many-electron states. This can be further illustrated by a simple estimate used in Ref. [33]. If we use the relativistic energy shifts calculated earlier for Yb⁺ [47] and the experimental energy interval between states 2

and 5, we get the correct value for the enhancement factor $K \sim -15$ without any new calculations for the neutral Yb.

The calculations in Ref. [33] for state 5 are performed with the use of the standard CI technique for 16 external electrons. Full-scale CI calculations in this case are not possible, because the CI matrix would be too large. In ref. [33] the problem is dealt with by drastically cutting the basis, leaving just two or three single-electron states in each partial wave up to g -wave. However, we have shown that up to twenty states in each partial wave are needed for basis saturation [48]. The significant cut of the basis leads to poor accuracy of the calculations. Ref. [33] admits that the energies are not reproduced well in the calculations (no numbers are given). As a result of their approximations, the accuracy for the transition amplitudes may also be poor.

V. FEASIBILITY CONSIDERATIONS

A. Light shifts

1. Lattice light shifts

Transitions involving states with nonzero electronic angular momentum are currently not employed for clock applications. Nevertheless, the first demonstration of spectroscopy of cold atoms in a lattice in the Lamb-Dicke regime was in fact performed on such a transition, $^1S_0 \rightarrow ^3P_1$ ($J_z = 0$) in bosonic ^{88}Sr [49]. The observed dependence of the light shifts on the polarization of the lattice wave was considered at the time to be an issue that would impede achieving ultrahigh accuracy and therefore this approach was not pursued further [24]. Work on lattice clocks has focused instead on $^1S_0 \rightarrow ^3P_0$ transitions, in several atomic species. However, one can argue that the issues arising from $J \neq 0$ clock states have not yet been fully explored. Here we propose an approach to control the light shifts.

Given the J_z -dependence of the light-atom interaction energy [24], we note that it is in principle possible to null the vector light shift, the tensor light shift and the first-order Zeeman shift and any static electric quadrupole shift by averaging over the 5 transitions $J_{z,b} = 0 \rightarrow J_{z,a} = 0, \pm 1, \pm 2$. This nulling is independent of the polarisation state of the lattice field. The magic wavelength is then determined by the vanishing of the difference of the scalar polarizabilities. Such a procedure would have to null rather large individual frequency shifts, therefore we consider only a single transition, to the $J_{z,a} = 0$ - state.

To second order in the electric field amplitude of the lattice field, the light shift of a transition $J_b = 0 \rightarrow J_a$ ($J_{z,a}$) is determined by the polarizability differ-

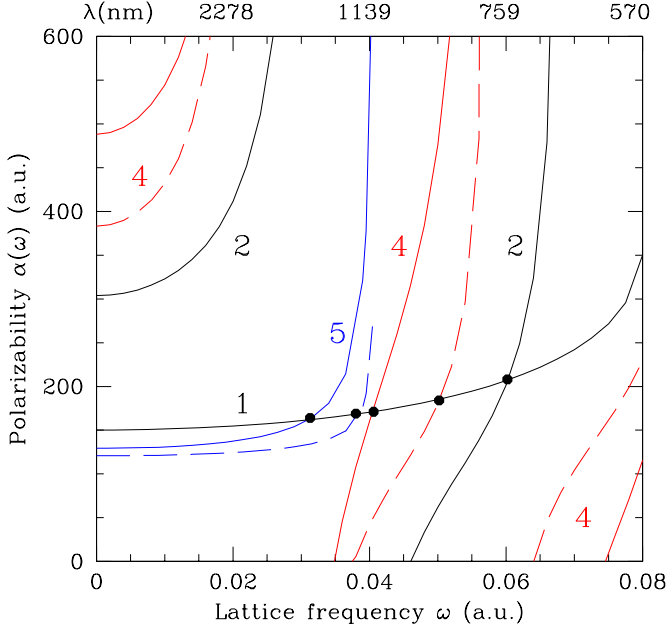


FIG. 2: Dynamic polarizabilities of clock states 1 (black), 2 (black), 4 (red) and 5 (blue). For states 4 and 5 it is assumed that the lattice laser polarization is linear and only states with $J_z = 0$ are considered. The solid line corresponds to laser polarization parallel to the magnetic field ($s^2 = 1$), and the dashed line to the polarization perpendicular to the magnetic field ($s^2 = 0$). Filled circles at line crossings indicate polarizabilities at magic frequencies (see Tab. VII). For state 5 the polarizabilities at $\omega > 0.04$ a.u. are not shown.

ence [24]

$$\Delta\alpha_{ab}(\omega_L) = \alpha_a^S(\omega_L) + \frac{1}{2}(3|\hat{\epsilon} \cdot \hat{B}|^2 - 1) \frac{3J_{z,a}^2 - J_a(J_a + 1)}{J_a(2J_a - 1)} \alpha_a^T(\omega_L) - \alpha_b^S(\omega_L). \quad (25)$$

Here, $\hat{\epsilon}$ is the polarization vector of the lattice laser. It is complex if the polarization has some degree of ellipticity. \hat{B} is the direction of the small magnetic field applied to split the transition, here into the five Zeeman components $J_{z,a} = 0, \pm 1, \pm 2$. Note that the above expression is simplified compared to the general expression [24] because the contribution of the vector polarizability is omitted. This is correct for an upper state with $J_{z,a} = 0$ or if the lattice wavevector is perpendicular to the magnetic field or if the lattice is linearly polarized.

Thus, for a given lattice frequency ω_L and a linearly polarized lattice, the polarizability difference depends on the experimentally adjustable parameter $s = \hat{\epsilon} \cdot \hat{B}$, the relative orientation between the lattice polarization and the quantization direction. As a consequence, there is no unique magic wavelength.

Hara et al [13] have performed a detailed experimental study of the light shift induced by an optical trap at the wavelength 1070 nm on the 1 - 4 ($J_{z,a} = 0, 1, 2$)

TABLE VII: Magic wavelengths of the transitions $J_b = 0 \rightarrow J_a = 2$, $J_{z,a} = 0$, for particular values of $s = \hat{\epsilon} \cdot \hat{B}$. $\alpha(\omega_{M,s})$ is the common polarizability for the state b and the state a . α_a^T is the tensor polarizability of the upper state.

Transition		$\omega_{M,s}$	$\lambda_{M,s}$	$\alpha(\omega_{M,s})$	$\alpha_a^T(\omega_{M,s})$
$b - a$	s^2	a.u.	cm ⁻¹	(nm)	(a.u.)
1 - 2		0.0602	13200	757	208
1 - 4	0	0.0502	11020	908	184
1 - 4	1	0.0406	8910	1122	171
1 - 5	0	0.0380	8340	1200	169
1 - 5	1	0.0313	6870	1460	164

transitions in bosonic ^{174}Yb . In particular, the authors discussed how to produce an "effective" magic trap for each $J_{z,a}$ state by adjusting s .

We now consider only the upper state $J_{z,a} = 0$ and a 1D lattice. Via adjustment of s it is possible to minimize (when $s = 0$) or maximize (when $s = 1$) the polarizability of this upper state, between the values $\alpha_{a,\min}(\omega_L) = \alpha_a^S(\omega_L) + \alpha_a^T(\omega_L)/2$ and $\alpha_{a,\max}(\omega_L) = \alpha_a^S(\omega_L) - \alpha_a^T(\omega_L)$, thus maximizing or minimizing the transition frequency. Here it is assumed that the lattice wavelength is larger than 800 nm, so that $\alpha_a^T(\omega_L) < 0$ for states 4 and 5. Note that $\alpha_{a,\max}(\omega_L)$ are given by the red and blue solid lines in Fig. 2 while curves for $\alpha_{a,\min}(\omega_L)$ are given by the red and blue dashed lines. The magic wavelengths are given in Table VII. The experimental value for the magic wavelength of the 1 - 2 transition is 759 nm [50], in good agreement with our computed 757 nm.

Ido and Katori [49] demonstrated a measurement of the transition frequency of Sr as a function of lattice wave polarization angle and observed a maximum and a minimum. Similar measurements were reported more recently for the $^1S_0 \rightarrow ^3P_2$ (i.e. 1 - 4) transitions of bosonic ^{174}Yb by Yamaguchi et al. [12]. In a $\lambda_L = 532$ nm optical trap, they measured the light shift both for $s = 1$ and for $s = 0$, nearly achieving a magic wavelength condition in the latter case.

We suggest that the transitions should be interrogated at the particular operating points $s = \hat{\epsilon} \cdot \hat{B} = 0$ or $s = \pm 1$, at the respective magic wavelengths $\omega_{M,s}$ which null the polarizability difference, $\Delta\alpha_{ab,s}(\omega_{M,s}) = 0$. These operating points have also been discussed by Westergaard et al [51] in the context of a fermionic lattice clock. Since the transition excitation radiation must propagate parallel to the lattice wave, and a π transition ($J_{z,b} = 0 \rightarrow J_{z,a} = 0$) is to be excited, a suitable geometry is (i) a magnetic field perpendicular to the lattice wave propagation and (ii) a linear lattice polarization, orthogonal ($s = 0$) or parallel ($s = 1$) to the magnetic field. These operating points provide extrema of the transition frequency, i.e. a quadratic dependence on the polarization setting, which is experimentally advantageous.

The operating points will be determined by extension of the well-known procedure of determining the "true" clock frequency corresponding to zero lattice intensity

[49]. For a given setting of s^2 , close to the maximum (1) or minimum (0) value, the clock frequency is measured as function of lattice laser intensity and as a function of detuning from the magic wavelength. This is repeated for different settings of s^2 and the extremum of the clock frequency is determined by a fit of expression (25) to the data. This is the "true", unperturbed frequency. s^2 can be varied by varying the polarisation direction or the magnetic field direction, or both.

The sensitivity of the transition frequency to s is

$$\delta(\Delta\omega_{LS}) = 0.7 \text{ kHz} \frac{\alpha_a^T(\omega_{M,s})}{1 \text{ a.u.}} \frac{I_M}{10 \text{ kW/cm}^2} \delta(s^2), \quad (26)$$

where I_M is the lattice intensity. If $\alpha_a^T \simeq 80 \text{ a.u.}$, a 1×10^{-18} fractional frequency shift is produced by a $\simeq 0.1 \text{ mrad}$ change in angle between $\hat{\epsilon}$ and \hat{B} around the operating points $s = 0, 1$ and for the reference intensity. This value is an estimate for the desirable stability of the angle over the course of the unperturbed-frequency-determination procedure and for the desirable linearity of the variation of the angle setting. Tab. VII indicates that the operating points $s = 1$ exhibit a moderately larger angle tolerance compared to $s = 0$, due to the former's smaller $|\alpha_a^T|$.

Evidently, in order to determine the optimum operation point accurately, not only the polarization optics should allow fine setability but also the intensity of the lattice should be stable over the course of the determination. Active stabilization of the lattice wave power and propagation direction can be helpful.

We consider this approach to be realistic, i.e. the unperturbed frequency can be determined in a reasonable total measurement duration, because of the low statistical uncertainty achievable with state-of-the-art clock lasers. We expect that the total uncertainty of the clock frequency related to the lattice shift only will be within a moderate factor of that achievable in conventional lattice clocks, where polarization optimization is not required.

A discussion of the atomic hyperpolarizability goes beyond the scope of this work. It is not possible to compute it accurately ab initio without experimental input data [52]. However, recent theoretical [53] and experimental work on the 1 - 2 transition in Yb [54] demonstrates that its effects can be precisely measured and controlled at the 10^{-18} level.

2. Probe light shift

The situation for the new transitions may be compared to that of the conventional transitions. In Yb on the 1 - 2 transition, a probe shift 0.8×10^{-18} and uncertainty of 3×10^{-18} has been reported [7]. In Sr, the probe shift coefficient is $-13 \text{ Hz cm}^2/\text{W}$ [55], similar to the Yb 1 - 2 transition. A shift 0.9×10^{-19} and an uncertainty of 0.5×10^{-19} have been achieved [7].

The probe shifts of the new transitions (1 - 4, 1 - 5) are estimated at $(0.05, 1) \times 10^{-19}$ for $T_\pi = 1 \text{ s}$ interrogation

time, using the coefficients given in Table IV. These shifts are comparable to those of the conventional transitions and therefore we expect that a similar uncertainty, in the 10^{-19} -range, should be achievable. The shifts and uncertainties can be further reduced by using longer atom interrogation times.

B. Zeeman shift

The experimental method typically used to determine the quadratic Zeeman (QZ) shift, yields an uncertainty proportional to the absolute value of the coefficient.

For the conventional 1 - 2 clock transition in Yb the uncertainty reported in [7] is 1×10^{-17} , where the shift coefficient is given in Tab. V, -0.06 Hz/G^2 . We can also quote results on ^{87}Sr , where on the similar transition uncertainties of $\approx 1 \times 10^{-18}$ [7, 56] have been reported, the coefficient being 4 times larger, -0.24 Hz/G^2 .

According to Tab. V, for the 1 - 4 (1 - 5) Yb transition, the QZ shift coefficient is approximately 5 (12) times smaller than for the 1 - 2 Yb transition. Compared to Sr, the Yb coefficients are 20 and 50 times smaller, respectively.

Thus, we expect that for the proposed transitions the uncertainty of the QZ shift can be reduced to the low- 10^{-19} range.

C. Cold collision shift

An important systematic effect in lattice clocks is collisional interactions between the ultra-cold atoms. In fermionic clocks these are effectively suppressed by using spin-polarized atoms, so that the Pauli principle forbids s-wave scattering [58]. For bosons, s-wave scattering is a relevant interaction, especially in a 1D lattice. The clock frequency must therefore be measured as a function of atom density, and the unperturbed clock frequency is determined by extrapolation.

The cold collision frequency shift is proportional to [59]

$$\rho(a_{aa} - a_{bb} + C'(a_{ab} - a_{bb} - a_{aa})), \quad (27)$$

where ρ is the atomic density, a_{ij} is the scattering length for the collision of an atom in state i and an atom in state j , and $C' \approx 0.5$ is a coefficient that depends on the excitation probability and other factors. Scattering lengths vary widely with mass and electronic state, and cannot be computed ab initio. The scattering length in the ground state, a_{bb} , has been measured for all Yb isotopes [57]. Concerning the $^3P_2(J_z = 0)$ state, for even isotopes only the value $a_{aa}(^{174}\text{Yb}) = -23 \text{ nm}$ [27, 60] is known so far (for a study of the fermion ^{171}Yb , see [15]). Thus, currently there is insufficient data for a prediction of the density shift of even a single bosonic isotope. No data exists related to level 5.

Nevertheless, it can be pointed out that there has recently been strong progress in the accuracy of bosonic

clocks using ^{88}Sr . Transition frequency uncertainties arising from cold collisions were measured to be equal to 11×10^{-18} [39] and 3×10^{-18} [41] fractionally. These clocks used 1D lattices and the technique of photoassociation to reduce the number of atoms in multiply occupied lattice sites. Also for the ^{88}Sr isotope not all scattering lengths are known. Therefore, no strong inference from the strontium clock performance to an Yb clock performance is possible. However, it is quite possible that some of the bosonic Yb isotopes have scattering lengths of similar size as or smaller than the ones of ^{88}Sr . Photoassociation in Yb is standard and has also been performed on the 1 - 4 transition [15].

The inelastic collision rate γ_{aa} between Yb atoms in the excited $^3\text{P}_2(J_z = 0)$ state is $\simeq 6 \times 10^{-11} \text{cm}^3 \text{s}^{-1}$ and, more importantly, much lower between ground-state and $^3\text{P}_2(J_z = 0)$ atoms, $\gamma_{ba} \simeq 1 \times 10^{-12} \text{cm}^3 \text{s}^{-1}$. Both were determined at $< 1 \mu\text{K}$ temperature [61]. In view of the values for ^{88}Sr [62], $\gamma_{aa} = (4.0 \pm 2.5) \times 10^{-12} \text{cm}^3 \text{s}^{-1}$ between atoms in the upper clock level $^3\text{P}_0$, and $\gamma_{ba} = (5.3 \pm 1.9) \times 10^{-13} \text{cm}^3 \text{s}^{-1}$ between in ground-state and excited-state atoms, the values for Yb do not seem problematic. Moreover, we note that the Yb values were measured in a crossed dipole trap, not in a lattice, and it has been observed for the case of Sr that lower values arise in a lattice [62].

D. Experimental implementation

Finally, we make a few comments on the implementation.

High-power, continuous-wave laser sources for the required magic wavelength lattices in the near-infrared spectral range are commercially available.

Controlling light shifts at the 10^{-18} level will require more effort than in the standard lattice clocks, but appears feasible.

The characterization of the systematic effects of the two new clock transitions can profit from the possibility to study both them and the standard clock transitions in the same apparatus, admitting a change of the lattice and clock lasers. In particular, this applies to the precise measurement of the black-body shift, which is dissimilar for the three transitions.

The preparation of the Yb atoms in the optical lattice can be implemented experimentally with the already well-established methods. That is, first and second-stage cooling can be performed with the standard 399 nm and 556 nm lasers and procedures. From the second-stage MOT, the atoms are released into a 1D lattice. The clock lasers (507 nm, 431 nm) excite the upper clock state via M2 excitation, which is possible, as was recently demonstrated for the 1 - 4 transition [12, 16, 61]. There is no difficulty in principle for realizing clock lasers for both transitions with ultra-narrow linewidth, using existing

technology.

The de-excitation of the atoms from the upper clock state (necessary for measuring the excitation produced by the clock laser) is already standard for state 4 as described in the cited references. For state 5 it could be done via excitation to states of the $4f^{14}6s6d$ configurations (using wavelengths $\sim 600 \text{nm}$) [38], which will subsequently decay in steps to the ground state.

VI. CONCLUSION.

We proposed two new clock states in bosonic Yb isotopes for use as clock transitions in an optical lattice clock for fundamental research. The transitions are from the ground state to metastable states with easily accessible excitation energies of 19710.388cm^{-1} and 23188.518cm^{-1} and angular momentum $J = 2$, $J_z = 0$.

The current main motivation to use these transitions is for a search for new physics beyond the Standard Model via the non-linearity of King's plot and via testing for a time drift or a time modulation of the ratio of the clock frequencies. It is very attractive that the time drift and modulation measurement could be performed with a single clock apparatus (with suitably extended laser system), similar to what is possible with the Yb^{3+} ion.

Both transitions have a clear potential for allowing to determine and control systematic shifts with high accuracy. Our analysis does not indicate clear obstacles towards reaching frequency uncertainty in the low 10^{-18} range. This level has already been achieved for the 1 - 2 transition at NIST. Thus, there are prospects of further improvements of the limits of the time variation on the fine structure constant, which currently stands at $\sim 10^{-17}$ per year [43–45].

Clearly, detailed experimental tests are required for investigating the validity of the proposed transitions in practice. This is especially so for the 1 - 5 transitions, which has not been studied experimentally yet. It seems that some key aspects of the present proposal can be characterized on existing clock devices with modest extensions. A measurement of the light shift will also be able to provide data allowing an estimate of the hyperpolarizabilities.

Acknowledgments

One of us (S.S.) approached M.S. Safronova with the idea of new Yb excited states for precision measurements. We thank her for suggesting S.S. to contact the other authors of this paper. S.S. acknowledges a helpful hint from A. Görlitz. This work was funded in part by the Australian Research Council and by project Schi 431/22-1 of the Deutsche Forschungsgemeinschaft.

-
- [1] A. D. Ludlow, M. M. Boyd, and J. Ye, *Rev. Mod. Phys.* **87**, 637 (2015).
- [2] C. W. Chou, D. B. Hume, J. C. J. Koelemeij, D. J. Wineland, and T. Rosenband, *Phys. Rev. Lett.* **104**, 070802 (2010).
- [3] N. Hinkley, J. A. Sherman, N. B. Phillips, et al. *Science* **341**, 1215 (2013).
- [4] K. Beloy, N. Hinkley, N. B. Phillips, et al. *Phys. Rev. Lett.* **113**, 260801 (2014).
- [5] I. Ushijima, M. Takamoto, M. Das, T. Ohkubo, and H. Katori, *Nature Photon.* **9**, 185 (2015).
- [6] T. L. Nicholson et al. *Nature Commun.* **6**, 6896 (2015).
- [7] N. Nemitz, T. Ohkubo, M. Takamoto, I. Ushijima, M. Das, N. Ohmae, and H. Katori, *Nature Photonics* **10**, 258 (2016).
- [8] V. V. Flambaum and V. A. Dzuba, *Can. J. Phys.* **87**, 25 (2009).
- [9] V. A. Dzuba, V. V. Flambaum, M. S. Safronova, S. G. Porsev, T. Pruttivarasin, M. A. Hohensee, H. Häffner, *Nature Physics* **12**, 465 (2016).
- [10] J. C. Berengut et al, arXiv:1704.05068 (2017).
- [11] V. V. Flambaum, A. J. Geddes, and A. V. Viatkina, *Phys. Rev. A* **97**, 032510 (2018).
- [12] A. Yamaguchi, S. Uetake, S. Kato, H. Ito and Y. Takahashi, *New Journal of Physics* **12**, 103001 (2010).
- [13] H. Hara, H. Konishi, S. Nakajima, Y. Takasu, and Y. Takahashi, *J. Phys. Soc. Jpn.* **83**, 014003 (2014).
- [14] S. Kato, K. Inaba, S. Sugawa, K. Shibata, R. Yamamoto, M. Yamashita, Y. Takahashi, *Nat. Comm.* **7**, 11341 (2016).
- [15] S. Taie, S. Watanabe, T. Ichinose, and Y. Takahashi *Phys. Rev. Lett.* **116**, 043202 (2016)
- [16] S. Kato, S. Sugawa, K. Shibata, R. Yamamoto, and Y. Takahashi, *Phys. Rev. Lett.* **110**, 173201 (2013).
- [17] V. A. Dzuba, J. C. Berengut, C. Harabati, and V. V. Flambaum, *Phys. Rev. A* **95**, 012503 (2017).
- [18] A. Kramida, Yu. Ralchenko, J. Reader, and NIST ASD Team (2018). NIST Atomic Spectra Database (ver. 5.5.2), [Online]. Available: <https://physics.nist.gov/asd> [2018, January 10]. National Institute of Standards and Technology, Gaithersburg, MD.
- [19] S. G. Porsev and A. Derevianko, *Phys. Rev. A* **69**, 042506 (2004).
- [20] Y. Takasu, K. Komori, K. Honda, M. Kumakura, T. Yabuzaki, and Y. Takahashi, *Phys. Rev. Lett.* **93**, 123202 (2004)
- [21] V. A. Dzuba and A. Derevianko, *J. Phys. B* **43**, 074011 (2010).
- [22] A. V. Taichenachev, V. I. Yudin, C. W. Oates, C. W. Hoyt, Z. W. Barber, and L. Hollberg, *Phys. Rev. Lett.* **96**, 083001 (2006).
- [23] V. A. Dzuba and V. V. Flambaum, *Phys. Rev. A* **93**, 052517 (2016).
- [24] A. Derevianko and H. Katori, *Rev. Mod. Phys.* **83**, 331 (2011).
- [25] V. A. Dzuba and V. V. Flambaum, *Hyperfine Interac* **237**, 160 (2016).
- [26] J. Mitroy, M. S. Safronova, and C. W. Clark, *J. Phys. B* **43**, 202001 (2010).
- [27] A. Yamaguchi, S. Uetake, D. Hashimoto, J. M. Doyle, and Y. Takahashi, *Phys. Rev. Lett.* **101**, 233002 (2008).
- [28] A. Khramov, A. Hansen, W. Dowd, R. J. Roy, C. Makrides, A. Petrov, S. Kotochigova, and S. Gupta, *Phys. Rev. Lett.* **112**, 033201 (2014).
- [29] J. A. Sherman, N. D. Lemke, N. Hinkley, M. Pizzocaro, R. W. Fox, A. D. Ludlow, and C. W. Oates, *Phys. Rev. Lett.* **108**, 153002 (2012).
- [30] V. A. Dzuba, A. Kozlov, and V. V. Flambaum, *Phys. Rev. A* **89**, 042507 (2014).
- [31] W. M. Itano, *J. Res. Natl. Inst. Stand. Technol.* **105**, 829 (2000).
- [32] N. D. Lemke, A. D. Ludlow, Z. W. Barber, T. M. Fortier, S. A. Diddams, Y. Jiang, S. R. Jefferts, T. P. Heavner, T. E. Parker, and C. W. Oates, *Phys. Rev. Lett.* **103**, 063001 (2009).
- [33] M. S. Safronova, S. G. Porsev, C. Sanner, and J. Ye, *Phys. Rev. Lett.* **120**, 173001 (2018).
- [34] V. A. Kostelecky and S. Samuel, *Phys. Rev. D* **39**, 683 (1989).
- [35] V. A. Dzuba and V. V. Flambaum, *Phys. Rev. D* **95**, 015019 (2017).
- [36] D. Colladay and V. A. Kostelecky, *Phys. Rev. D* **58**, 116002 (1998).
- [37] T. Pruttivarasin, M. Ramm, S. G. Porsev, I. I. Tupitsyn, M. S. Safronova, M. A. Hohensee, and H. Häffner, *Nature* **517**, 592 (2015).
- [38] W.-G. Jin, T. Horiguchi, M. Wakasugi, T. Hasegawa, W. Yang, *J. Phys. Soc. Japan* **60**, 2896 (1991).
- [39] T. Takano, R. Mizushima, and H. Katori, *Applied Physics Express* **10**, 072801 (2017).
- [40] C. Radzewicz, M. Bober, P. Morzynski, A. Cygan, D. Lisak, D. Bartoszek-Bober, P. Maslowski, P. Ablewski, J. Zachorowski, W. Gawlik, R. Ciurylo and M. Zawada, *Phys. Scr.* **91** (2016) 084003
- [41] S. Origlia et al, arXiv:1803.03157v1.
- [42] V. A. Dzuba and V. V. Flambaum, *Phys. Rev. A*, **77**, 012515 (2008).
- [43] N. Leefer, C. T. M. Weber, A. Cingöz, J. R. Torgerson, and D. Budker, *Phys. Rev. Lett.* **111**, 060801 (2013).
- [44] T. Rosenband, D. B. Hume, P. O. Schmidt, C. W. Chou, A. Brusch, L. Lorini, W. H. Oskay et al, *Science* **319**, 1808 (2008).
- [45] R. M. Godun, P. B. R. Nisbet-Jones, J. M. Jones, S. A. King, L. A. M. Johnson, H. S. Margolis, K. Szymaniec, S. N. Lea, K. Bongs, and P. Gill, *Phys. Rev. Lett.* **113**, 210801 (2014).
- [46] V. A. Dzuba, V. V. Flambaum, and J. K. Webb, *Phys. Rev. A* **59**, 230 (1999).
- [47] V. A. Dzuba and V. V. Flambaum, *Phys. Rev. A* **77**, 012515 (2008).
- [48] V. A. Dzuba, M. S. Safronova, U. I. Safronova, and A. Kramida, *Phys. Rev. A* **94**, 042503 (2016).
- [49] T. Ido and H. Katori, *Phys. Rev. Lett.* **91**, 053001 (2003).
- [50] Z. W. Barber, J. E. Stalnaker, N. D. Lemke, N. Poli, C. W. Oates, T. M. Fortier, S. A. Diddams, L. Hollberg, C. W. Hoyt, A. V. Taichenachev, and V. I. Yudin, *Phys. Rev. Lett.* **100**, 103002 (2008).
- [51] P. G. Westergaard, J. Lodewyck, L. Lorini, A. Lecallier, E. A. Burt, M. Zawada, J. Mollo, and P. Lemonde, *Phys. Rev. Lett.* **106**, 210801 (2011)
- [52] S. G. Porsev, A. Derevianko, E. N. Fortson, *Phys. Rev. A* **69**, 021403(R) (2004).

- [53] H. Katori, V. D. Ovsiannikov, S. I. Marmo, V. G. Palchikov, Phys. Rev. A **91**, 052503 (2015)
- [54] R. C. Brown, N. B. Phillips, K. Beloy, W. F. McGrew, M. Schioppo, R. J. Fasano, G. Milani, X. Zhang, N. Hinkley, H. Leopardi, T. H. Yoon, D. Nicolodi, T. M. Fortier, A. D. Ludlow, Phys. Rev. Lett. **119**, 253001 (2017)
- [55] X. Baillard, M. Fouch, R. Le Targat, P. Westergaard, A. Lecallier, Y. Le Coq, G. D. Rovera, S. Bize, and P. Lemonde, Opt. Lett. **32**, 1812 (2007)
- [56] S. Falke *et al.*, New J. Phys. **16**, 073023, (2014)
- [57] M. Kitagawa, K. Enomoto, K. Kasa, Y. Takahashi, R. Ciurylo, P. Naidon, and P.S. Julienne, Phys. Rev. A **77**, 012719 (2008).
- [58] M. Takamoto, F.-L. Hong, R. Higashi, Y. Fujii, M. Imae, and H. Katori, J. Phys. Soc. Japan **75**, 104302 (2006).
- [59] D. M. Harber, H. J. Lewandowski, J. M. McGuirk, and E. A. Cornell, Phys. Rev. A **66**, 053616 (2002).
- [60] M Yamashita, S. Kato, A. Yamaguchi, S. Sugawa, T. Fukuhara, S. Uetake, and Y. Takahashi, Phys. Rev. A **87**, 041604(R) (2013).
- [61] S. Uetake, R. Murakami, J.M. Doyle, and Y. Takahashi, Phys. Rev. A **86**, 032712 (2012).
- [62] Ch. Lisdar, J. S. R. Vellore Winfred, T. Middelmann, F. Riehle, and U. Sterr, Phys. Rev. Lett. **103**, 090801 (2009)